# GaSb-based mid infrared photonic crystal surface emitting lasers

**Chien Hung Pan,[1,2,*] Chien Hung Lin,[2] Ting Yuan Chang,[3] Tien Chang Lu,[3] and Chien Ping Lee[2]**

[1]*Center for Nano Science and Technology, National Chiao Tung University, 1001 University Road, Hsinchu 30010, Taiwan*
[2]*Department of Electronics Engineering and Institute of Electronics, National Chiao Tung University, 1001 University Road, Hsinchu 30010, Taiwan*
[3]*Department of Photonics and Institute of Electro-Optical Engineering, National Chiao Tung University, 1001 University Road Hsinchu 30010, Taiwan*
[*]*panjoan.ee95g@g2.nctu.edu.tw*

**Abstract:** We demonstrated for the first time above room temperature (RT) GaSb-based mid-infrared photonic crystal surface emitting lasers (PCSELs). The lasers, under optical pumping, emitted at $\lambda_{lasing} \sim 2.3 \mu m$, had a temperature insensitive line width of 0.3nm, and a threshold power density ($P_{th}$) ~0.3KW/cm$^2$ at RT. Type-I InGaAsSb quantum wells were used as the active region, and the photonic crystal, a square lattice, was fabricated on the surface to provide optical feedback for laser operation and light coupling for surface emission. The PCSELs were operated at temperatures up to 350K with a small wavelength shift rate of 0.21 nm/K. The PCSELs with different air hole depth were studied. The effect of the etched depth on the laser performance was also investigated using numerical simulation based on the coupled-wave theory. Both the laser wavelength and the threshold power decrease as the depth of the PC becomes larger. The calculated results agree well with the experimental findings.

## References and links

1. A. Joullié and P. Christol, "GaSb-based mid-infrared 2−5 µm laser diodes," C. R. Phys. **4**(6), 621–637 (2003).
2. S. Schilt, A. Vicet, R. Werner, M. Mattiello, L. Thévenaz, A. Salhi, Y. Rouillard, and J. Koeth, "Application of antimonide diode lasers in photoacoustic spectroscopy," Spectrochim. Acta A Mol. Biomol. Spectrosc. **60**(14), 3431–3436 (2004).
3. Z. Yin and X. Tang, "A review of energy bandgap engineering in III–V semiconductor alloys for mid-infrared laser applications," Solid-State Electron. **51**(1), 6–15 (2007).
4. J. Seufert, M. Fischer, M. Legge, J. Koeth, R. Werner, M. Kamp, and A. Forchel, "DFB laser diodes in the wavelength range from 760 nm to 2.5 µm," Spectrochim. Acta A Mol. Biomol. Spectrosc. **60**(14), 3243–3247 (2004).
5. S. H. Macomber, J. S. Mott, R. J. Noll, G. M. Gallatin, E. J. Gratrix, S. L. O'Dwyer, and S. A. Lambert, "Surface-emitting distributed feedback semiconductor laser," Appl. Phys. Lett. **51**(7), 472–474 (1987).
6. R. J. Noll and S. H. Macomber, "Analysis of grating surface emitting lasers," IEEE J. Quantum Electron. **26**(3), 456–466 (1990).
7. M. Imada, S. Noda, A. Chutinan, T. Tokuda, M. Murata, and G. Sasaki, "Coherent two-dimensional lasing action in surface-emitting laser with triangular-lattice photonic crystal structure," Appl. Phys. Lett. **75**(3), 316–318 (1999).
8. S. Noda, M. Yokoyama, M. Imada, A. Chutinan, and M. Mochizuki, "Polarization mode control of two-dimensional photonic crystal Laser by unit cell Structure Design," Science **293**(5532), 1123–1125 (2001).
9. M. Imada, A. Chutinan, S. Noda, and M. Mochizuki, "Multidirectionally distributed feedback photonic crystal lasers," Phys. Rev. B **65**(19), 195306 (2002).
10. I. Vurgaftman and J. R. Meyer, "Design optimization for high-brightness surface-emitting photonic-crystal distributed-feedback lasers," IEEE J. Quantum Electron. **39**(6), 689–700 (2003).

11. M. Lu, S. S. Choi, C. J. Wagner, J. G. Eden, and B. T. Cunningham, "Label free biosensor incorporating a replica-molded, vertically emitting distributed feedback laser," Appl. Phys. Lett. **92**(26), 261502 (2008).
12. T.-C. Lu, S.-W. Chen, T.-T. Kao, and T.-W. Liu, "Characteristics of GaN-based photonic crystal surface emitting lasers," Appl. Phys. Lett. **93**(11), 111111 (2008).
13. C. Ge, M. Lu, W. Zhang, and B. T. Cunningham, "Distributed feedback laser biosensor incorporating a titanium dioxide nanorod surface," Appl. Phys. Lett. **96**(16), 163702 (2010).
14. M. Kanskar, J. Cai, D. Kedlaya, D. Olson, Y. Xiao, T. Klos, M. Martin, C. Galstad, and S. H. Macomber, "High-brightness 975-nm surface-emitting distributed feedback laser and arrays," Proc. SPIE **7686**, 76860J (2010).
15. Y. Liang, C. Peng, K. Sakai, S. Iwahashi, and S. Noda, "Three-dimensional coupled-wave model for square-lattice photonic crystal lasers with transverse electric polarization: A general approach," Phys. Rev. B **84**(19), 195119 (2011).
16. E. Mujagić, C. Schwarzer, Y. Yao, J. Chen, C. Gmachl, and G. Strasser, "Two-dimensional broadband distributed-feedback quantum cascade laser arrays," Appl. Phys. Lett. **98**(14), 141101 (2011).
17. Y. Liang, C. Peng, K. Sakai, S. Iwahashi, and S. Noda, "Three-dimensional coupled-wave analysis for square-lattice photonic crystal surface emitting lasers with transverse-electric polarization: finite-size effects," Opt. Express **20**(14), 15945–15961 (2012).
18. K. Hirose, Y. Liang, Y. Kurosaka, A. Watanabe, T. Sugiyama, and S. Noda, "Watt-class high-power, high-beam-quality photonic-crystal lasers," Nat. Photonics **8**(5), 406–411 (2014).
19. J. S. Mott and S. H. Macomber, "Two-dimensional surface emitting distributed feedback laser arrays," IEEE Photon. Technol. Lett. **1**(8), 202–204 (1989).
20. A. Bauer, K. Rößner, T. Lehnhardt, M. Kamp, S. Höfling, L. Worschech, and A. Forchel, "Mid-infrared semiconductor heterostructure lasers for gas sensing applications," Semicond. Sci. Technol. **26**(1), 014032 (2011).
21. M. Kim, C. S. Kim, W. W. Bewley, J. R. Lindle, C. L. Canedy, I. Vurgaftman, and J. R. Meyer, "Surface-emitting photonic-crystal distributed-feedback laser for the midinfrared," Appl. Phys. Lett. **88**(19), 191105 (2006).
22. M. Jahjah, A. Vicet, and Y. Rouillard, "A QEPAS based methane sensor with a 2.35 μm antimonide laser," Appl. Phys. B **106**(2), 483–489 (2012).
23. A. Salhi, D. Barat, D. Romanini, Y. Rouillard, A. Ouvrard, R. Werner, J. Seufert, J. Koeth, A. Vicet, and A. Garnache, "Single-frequency Sb-based distributed-feedback lasers emitting at 2.3 μm above room temperature for application in tunable diode laser absorption spectroscopy," Appl. Opt. **45**(20), 4957–4965 (2006).
24. R. M. Briggs, C. Frez, M. Bagheri, C. E. Borgentun, J. A. Gupta, M. F. Witinski, J. G. Anderson, and S. Forouhar, "Single-mode 2.65 μm InGaAsSb/AlInGaAsSb laterally coupled distributed-feedback diode lasers for atmospheric gas detection," Opt. Express **21**(1), 1317–1323 (2013).
25. C.-H. Lin and C.-P. Lee, "Enhanced optical property in quaternary GaInAsSb/AlGaAsSb quantum wells," J. Appl. Phys. **116**(15), 153504 (2014).
26. K. Sakai, E. Miyai, and S. Noda, "Coupled-wave theory for square-lattice photonic crystal lasers with TE polarization," IEEE J. Quantum Electron. **46**(5), 788–795 (2010).

## 1. Introduction

GaSb-based material system is very important in the 2-5 μm mid-infrared (mid-IR) range for gas and chemical sensing such as in bio-medical industry and environment monitoring [1–4]. Reliable light sources in this wavelength range operating at room temperature with narrow line width and good beam quality are thus required. For this purpose, various GaSb based lasers have been developed.

Forming a resonant cavity with desired output bean quality is one of the most important factors in determining a laser's quality. For the mid-IR applications, it is especially true because the wavelength stability and purity as well as the beam divergence angle and the control of directionality are all important in real applications. Asides from the conventional Fabry-Perot cavities, cavities formed by photonic crystal often provide a better solution for the requirements mentioned above. Photonic crystal structures with surface emitting capabilities are particularly attractive because of the convenience of use and the easy integration with other devices.

Photonic crystal surface emitting lasers (PCSELs) have been around for quite some time [5–21] in both the one dimensional (1D) and the two dimensional (2D) designs. By proper design of the optical lattice for certain Bragg condition, the artificial photonic crystal forms a resonant cavity for laser oscillation and at the same time couples the laser light out of the surface. PCSELs have lots of advantages such as high output power [14, 18], narrow line width [7], good beam quality and controllability [8, 10], and 2D array arrangement capability [16, 19].

Although photonic crystal has been widely used in GaAs and InP-based lasers, there are very limited reports on GaSb based devices. To our knowledge there was only one previous work on GaSb-based mid-IR PCSELs, which, however, were operable only at low temperatures [21]. In this work, we report for the first time above room temperature operation of GaSb PCSELs by optical pumping. The emitting wavelength was 2.3μm, which could be useful for CO, $CH_4$ and $NH_3$ detections [2, 22].

## 2. Experiments

The sample used in this study was grown by a VEECO GEN-II molecular beam epitaxy system. The devices had a separate confinement hetero-structure (SCH) described as follows: On an n + GaSb (001) substrate, a 2.3μm-thick $Al_{0.85}Ga_{0.15}As_{0.07}Sb_{0.93}$ bottom-cladding layer was first grown. It was followed by a 150nm-thick $Al_{0.3}Ga_{0.7}As_{0.02}Sb_{0.98}$ waveguide layer. An active region was grown next. It consisted of four stacks of 12nm/ 25nm $In_{0.35}Ga_{0.65}As_{0.14}Sb_{0.86}$/ $Al_{0.3}Ga_{0.7}As_{0.02}Sb_{0.98}$ quantum well (QW)/ barrier structures. Another 200nm-thick $Al_{0.3}Ga_{0.7}As_{0.02}Sb_{0.98}$ waveguide layer was grown, which was then followed by a 200nm-thick $Al_{0.5}Ga_{0.5}As_{0.04}Sb_{0.96}$ top-cladding layer. The whole structure was then capped by a 20nm GaSb layer. Note that we designed the top-cladding layer with less aluminum mole faction as compared to bottom-cladding layer. It helps the guided mode leak out to the top surface due to the higher refractive index, and provides better wave coupling to the PC region. Another reason is to prevent it from possible oxidation, which could degrade the device performance.

After the growth the sample was deposited with a layer of 50nm thick $Si_3N_4$ by plasma enhanced chemical vapor deposition (PECVD) as a hard mask for the subsequent dry etching process. Our photonic crystal pattern was designed for the transverse electric (TE) mode in a square lattice operated at Γ1 band edge, which had a period (p) of 650 nm and round shaped air-holes with a filling factor of 0.12, defined as the hole area/ $p^2$ ratio. The photonic crystal was defined by e-beam lithography and etched by an inductively coupled plasma- reactive ionic etching (ICP-RIE) system. The devices had a size of 200μm x 200μm.

Because of the symmetry of PC patterns, there are four in-plane waves at Γ1 band edge coupled together, with their wave vector magnitude $k_i \sim G_1$, where $G_1 = 2\pi/p$ is the reciprocal lattice spacing of the PC. The emitting laser light has the wave vector $k_d$ normal to the surface.

The schematic diagram of the PCSEL together with the laser epi-structure and the scanning electron microscope (SEM) top view of the PC pattern are shown in Fig. 1. We fabricated two PCSELs with different etched depths for the air holes. Sample A had an etched depth of 170 nm while sample B had an etched depth of 220nm.
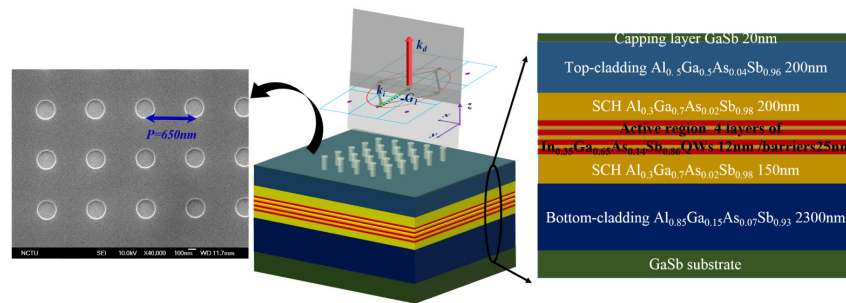


Fig. 1. The schematic diagram of PCSELs (middle), the laser epi-structure (right), and the SEM top view of the PC pattern (left). The PC pattern is a square lattice (650 nm period) with the round shape air-holes (0.12 filling factor). Four coupled in-plane waves are represented by green arrows, with the wave vector magnitude $k_i \sim G_1 = 2\pi/p$ (the PC reciprocal lattice). The surface emitting wave ($k_d$) is represented by the red arrow with a normal angle to the surface.

The fabricated PCSELs were glued on a copper chuck with thermal grease, and the temperature was controlled by a thermoelectric cooler. The excitation source was a pulsed fiber laser with a wavelength of 1064nm, a pulse width of 100 ns, and a repetition rate of 5K Hertz. A CaF$_2$ lens with a focal length of 4cm was used to focus the normally incident pump beam onto the surface of the device. The resulted spot size diameter was around 200μm. The objective lens was also used to collect the mid-IR light from the PCSELs. The collected light went through a long pass filter and then a CaF$_2$ lens for focusing. A 0.32 meter Czerny-Turner monochromator and a thermoelectric cooled InGaAsSb detector were used to disperse and detect the mid-IR spectrum of the light. A conventional lock-in amplify technique was used to analyze the signal.

## 3. Results and discussions

The lasing characteristics of the two PCSELs were studied at different temperatures varying from 290K to 350K in steps of 10K. Figure 2(a) shows the output power vs. input power plot (L-L plot) of sample A. The spectra of the same device operated at $1.4P_{th}$ and different temperatures are shown in Fig. 2(b). The laser behaved very well throughout the temperature range. The spectra showed a full width of half maximum (FWHM) of 0.3nm throughout the temperatures. This is much better than that of conventional Fabry-Perot (FP) lasers, which typically have multi-modes and much wider spectra. The line width is comparable to that of the only previous work on GaSb-based PCSELs [21], which had a FWHM of 0.13nm under CW optical pumping at 81K. Compared to conventional DFB lasers [23], the linewidth of our PCSELs is significantly wider. It could be due to the very narrow and low duty cycle pumping pulses used in the experiment and the non-uniformity of the 2D etched photonic crystal. The observed side mode suppression ratio (SMSR) for our devices was more than 27dB, which was limited by the noise of the detector used. The characteristics of sample B behaved very similarly and are not shown here.
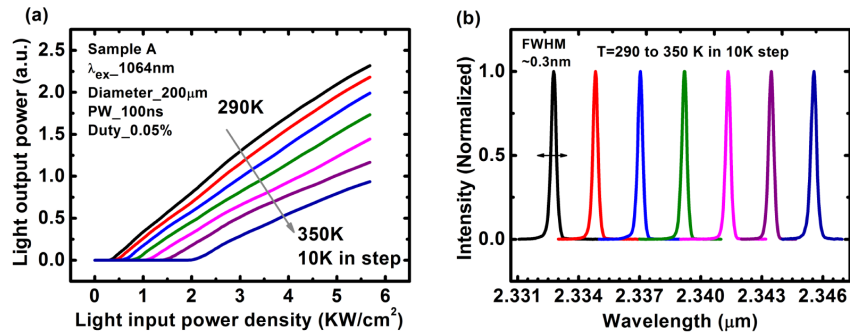


Fig. 2. The sample A (a) light in-light out curves and (b) lasing spectra with temperature varied from 290K to 350K in steps of 10K.

Figure 3 (a) and 3(b) show, respectively, the lasing wavelengths ($\lambda_{lasing}$) and threshold pumping power densities ($P_{th}$) as functions of temperature for both samples. Sample B, which had a deeper etch for the air holes, had a slightly shorter lasing wavelength than sample A, but with a much lower threshold pumping power. This is due to the stronger coupling of the diffracted light waves because the deeper etched holes. The lasing wavelength was about 2330nm at 290K. The temperature dependence was very weak with a red shift rate of 0.21 nm/K as the temperature increased. This value is similar to what was reported for GaSb-based DFB lasers [20,24] and is much lower than that of conventional Fabry-Perot (FP) lasers. For comparison, we also fabricated an edge-emitting Fabry Perot (FP) laser with a cavity length of 800 μm from the same material and also operated with optical pumping. The measured wavelength, shown as the dashed line in Fig. 2, shifted with temperature at a rate of 1.62 nm/K, which is about 8 times larger than that of the PCSELs. The temperature insensitivity of

the lasing wavelength is because the resonant condition is determined by the Bragg condition, which has a low temperature sensitivity as compared to the material's band gap energy, which is the dominating factor in determining the laser wavelength with a conventional cavity.

Both devices could be easily operated up to 350K, at which sample A had a lasing wavelength of 2345.6 nm. This is the record high operating temperature ever reported for a photonic crystal GaSb laser operating at such wavelength. We attribute the high temperature operation capability to the excellent material quality of our samples. The MBE growth technique we developed recently has eliminated the localized states problem, which often plagued the Sb compounds and heterostructures, and greatly improved the quality of the QWs and the barrier layers in our samples [25].

The threshold pumping powers ($P_{th}$) for samples A and B were 0.35 KW/cm$^2$ and 0.26 KW/cm$^2$ at 290K, respectively. They increased to 2.06 KW/cm$^2$ and 1.46 KW/cm$^2$ at 350K. The semi-log plot, shown in Fig. 3(b), of $P_{th}$ vs. temperature shows a well behaved exponential dependence. Fitting the experimental data with the relation, $P_{th} \sim e^{T/T0}$, we obtain an extracted characteristic $T_0$ value of 34K. For the FP laser, however, the extracted $T_0$ was 67K as shown by the fitted dash line in Fig. 3(b). The $T_0$ value for our FP laser was comparable to the recent reported results [20]. The possible reason for the lower $T_0$ value of the PCSELs is the increase of mismatch between the lasing wavelength and the gain peak of the QWs as the temperature rises. We can see, from Fig. 3(a), the difference in $\lambda_{lasing}$ between the PCSELs and the FP laser increases from ~50nm at 290K to a value of ~140nm at 350K. The increase of $\Delta\lambda_{lasing}$ indicates that the resonant wavelength of the photonic crystal moves away from the material's gain peak as the temperature is increased. This, however, can be improved if we fabricate the photonic crystal with a longer resonant wavelength compared to the gain peak at room temperature. Since the gain peak moves faster than the resonant wavelength as the temperature changes, the mismatch between the two will be reduced as temperature rises and could provide a large characteristic $T_0$ for the operation near room temperature. Figure 3(c) shows the temperature dependence of the laser's slope efficiency ($\eta$). Both lasers have the similar behavior. By fitting the data with $\eta \sim e^{-T/T1}$, we extracted a $T_1$ value of 88K. From 290K to 350K, there is only about 50% drop in the efficiency.

We have also estimated the divergent angle of the output beam by scanning the lasing intensity over the horizontal plane, which was 25cm away from the PCSELs. The divergent angle, extracted from the tangent geometry relationship, of overall light cone area was within 2 degrees. This is an order of magnitude better than that of conventional FP or edge emitting lasers.
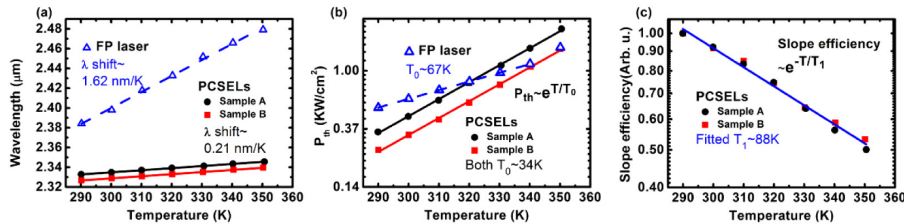


Fig. 3. The temperature dependent characteristics of PCSELs for sample A (170 nm etching depth) and sample B (220 nm etching depth) with solid symbols. Temperature dependence of (a) lasing wavelength ($\lambda_{lasing}$), (b) threshold pumping power density ($P_{th}$), and (c) slope efficiency, where solid lines are fitted curves. For comparison, an optically pumped FP laser with 0.8 mm cavity length shown with open symbols and dash fitted curves.

In order to evaluate the influence of the depth of the etched air holes on the PCSELs performance, we have developed a model for simulations. The layer thicknesses (d) and their refractive indices (n) are listed in Table 1, where the parameters were based on the epi structure used in our devices. The active region, which consists of four QWs and the in between spacer layers was treated as a single layer with a total thickness of 123nm. The

etched air hole depth, x, also defines the PC region and the thickness of the top-cladding layer. The model was based on the 3D coupled-wave theory published before [17, 26]. Figure 4 displays the vertical distribution of the calculated TE mode electric field (the right y-axis) and the refraction index of the structure (the left y-axis) for the case of a 170nm etched depth.

**Table 1. The layer thickness (d) and the refraction index (n) of the PCSELs model structure for the simulations**

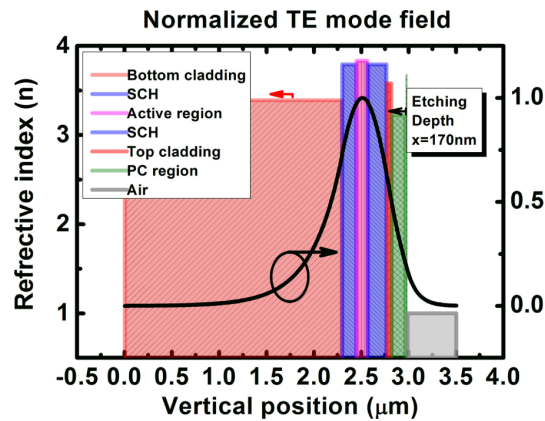| Model structure | Layer thickness d(nm) | Refractive index N |
|---|---|---|
| Air | 500 | 1 |
| PC region (etching depth x) | 20 | 3.68 |
| | x-20 | 3.42 |
| Top cladding | 220-x | 3.58 |
| SCH layer | 200 | 3.79 |
| Active region | 123 | 3.83 |
| SCH layer | 150 | 3.79 |
| Bottom cladding | 2300 | 3.39 |



Fig. 4. The refractive index of the model structure (left-axis) and the normalized TE mode field (right-axis) vertical distributions for the simulation case (etching depth x = 170nm). The layers were presented with different colors for better understanding of the overlap between electric field and active (and PC) region.

The simulation results of the lasing wavelength and the threshold gain as functions of the etched depth are shown in Fig. 5(a) and 5(b) respectively. The lasing wavelength shifts to a shorter wavelength when the etching depth is increased. This is the result of the effect of effective refractive index ($n_{eff}$) on the PCSELs' resonance condition, $\lambda_{lasing} /n_{eff} \sim p$. The $n_{eff}$ of the lasing mode is a function of the etched depth. When the etched depth increases, the optical field penetrates more into the PC region, where the refractive index is lower. So the effective mode index, $n_{eff}$, decreases, and hence the lasing wavelength decreases in order to satisfy the Bragg condition. The measured data (shown as open dots) agree well with the calculated results. We also notice that this effect gets stronger as the etched depth gets closer to the waveguide. Deeper etched holes also enhance the coupling of the horizontal traveling waves. So the threshold gain for the laser drops, as shown in Fig. 5(b). This explains why the measured threshold power density drops as the depth of the air holes increases. This tendency is similar to 1D DFB laser [6].
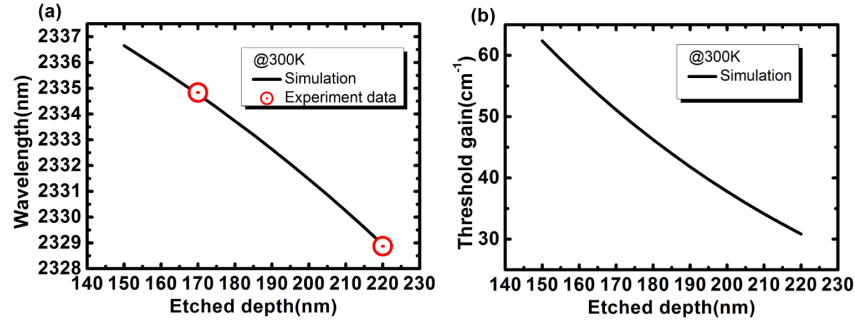
Fig. 5. Simulation results of (a) $\lambda_{lasing}$ and (b) threshold gain versus etched depth in the solid lines, and the experiment data shown with the open symbols, where the $P_{th}$ correlated to the threshold gain on the right axis in (b).

## 4. Conclusion

In conclusion, we successfully demonstrated above room temperature operation of optically pumped GaSb-based surface emitting photonic crystal lasers with a wavelength around 2.3μm. The emitted light had a nearly temperature independent line width of 0.3nm. The threshold power density was 0.3 KW/cm$^2$ at RT. The PCSELs consisted four layers of $In_{0.35}Ga_{0.65}As_{0.14}Sb_{0.86}/Al_{0.3}Ga_{0.7}As_{0.02}Sb_{0.98}$ type-I quantum wells, and the photonic crystal had a square lattice with circular air-holes spaced at 650nm from each other. The filling factor was 0.12. Two PCSELs with different etched depth for the air holes were studied with temperature varied from 290K to 350K. The lasing peak wavelength showed a red shift rate of 0.21nm/K, which is about eight times smaller than a conventional FP laser. The beam divergence angle was within 2 degrees. We simulated the influence of the etched depth on the performance of the PCSELs using the 3D coupled-wave theory. A good agreement between the calculation and the experimental results was obtained. The high temperature operation and the good beam quality make the PCSELs very attractive for mid-infrared applications.